Photodiagnosis and Photodynamic Therapy 37 (2022) 102711

Contents lists available at ScienceDirect

Photodiagnosis and Photodynamic Therapy

journal homepage: www.elsevier.com/locate/pdpdt

Fluorescence spectrometry based chromaticity mapping, characterization, and quantitative assessment of dental caries

Cheng Wang [a,c], Rongjun Zhang [a], Yongfu Jiang [a,b], Jiayang Li [a,b], Nizhou Liu [a,b], Le Wang [a], Peiyu Wu [d], Junbo He [a], Qi Yao [a,c,*], Xiaoling Wei [a,b,**]

[a] Department of Optical Science and Engineering, School of Information Science and Technology, Academy for Engineering and Technology, Shanghai Stomatological Hospital, Fudan University, Shanghai, China
[b] Shanghai Key Laboratory of Craniomaxillofacial Development and Diseases, Fudan University, Shanghai, China
[c] State Key Laboratory of Applied Optics, Changchun Institute of Optics, Fine Mechanics and Physics, Chinese Academy of Sciences, Changchun, China
[d] College of Architecture and Urban Planning, Shenzhen University, Guangdong, China

ARTICLE INFO

Keywords:
Chromaticity coordinates
Dental caries
Fluorescence spectroscopy
Hyperspectral imaging
Neural network fitting, Spectral area ratio

ABSTRACT

Purpose: Dental caries detection, especially the accurate detection of early caries, facilitates prompt interventions. It is reasonably common to use fluorescence imaging for classification and evaluation of caries, but lacks a quantitative, precise and easy-to-use characterization for practical applications. In this study a quantitative approach for caries stage detection by correlating caries spectral and chromatic features was examined.
Methods: A 405 nm LED light source was used as the excitation source. A hyperspectral imaging camera is employed to collect 336 spectral data of different caries stages. Four critical intervals for different stages of caries were extracted by fluorescence spectral features. The mapping relationship between caries spectral and chromatic features was established by Fast Formula Fitting (FFF) and Neural Network Fitting (NNF) methods.
Results: The 470–780 nm spectral power distribution was proved to be the best matching color waveband guiding the selection of filters in future instrument development. The correlation coefficients for the two fitting methods were 0.990 and 0.999, respectively. Both methods achieved caries stage prediction at the pixel level with high accuracy using color information. The visualization region in the chromaticity diagram was created.
Conclusions: This quantitative method enables accurate prediction of caries on the entire tooth surface and facilitates the development of portable and low-cost caries detection instruments.

1. Introduction

Dental caries, also known as tooth decay, is considered one of the most widespread oral diseases, which involves interactions between the tooth structure, the microbial biofilm formed on the tooth surface and sugars, as well as salivary and genetic influences [1,2]. The Global Burden of Disease Study revealed that dental caries are highly prevalent, affecting approximately 3.9 billion people worldwide, including 60–90% of school children and most adults [3]. The dynamic caries process consists of rapidly alternating periods of tooth demineralization and remineralization, leading to caries lesions in some anatomical regions of the tooth if net demineralization occurs over a sufficiently long time [1]. In clinical practice, dentists have relied on visual inspection, probes, and radiographs to identify caries [4]. Diagnosis based on radiological examination is also reliable for caries infections that have extended to the dentin layer, but at this stage, the main treatment option is to drill and fix them with restorative materials [5]. If early caries can be detected before caries formation, the disease progression can be contained and reversed with non-invasive remineralization treatment [6]. Optical and imaging-based methods have been lately increasingly applied for the early detection of caries lesions, including Optical Coherence Tomography (OCT), Near-infrared digital imaging transillumination, LED fluorescence, Polarized Raman spectroscopy, multiphoton imaging, and Laser fluorescence (LF) [7–10].

Fluorescence spectroscopy, including LED fluorescence and LF, is a non-invasive, non-ionized probing process, showing high sensitivity and specificity. At specific violet-blue wavelengths, normal dental tissues have the optical property of autofluorescence emission [11]. In addition,

* Corresponding author at: Academy for Engineering and Technology, Fudan University, Shanghai 200433, China.
** Co-corresponding author at: Department of Endodontics, Shanghai Stomatological Hospital, Fudan University, Shanghai 200001, China.
E-mail addresses: yaoqi@fudan.edu.cn (Q. Yao), xiaoling_wei@fudan.edu.cn (X. Wei).

https://doi.org/10.1016/j.pdpdt.2021.102711
Received 22 October 2021; Received in revised form 29 December 2021; Accepted 30 December 2021
Available online 2 January 2022

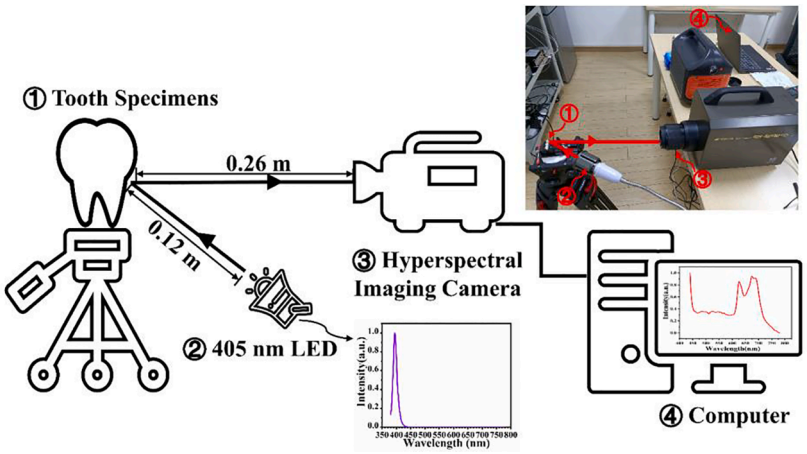

Fig. 1. Schematic diagram of the experimental procedure.

the fluorescence emission spectra of carious lesions contain additional emission peaks at 590–700 nm (red part), which are not observed in healthy tissues [12]. This red fluorescence, which may probably originate from porphyrins produced during bacterial metabolites, can be employed to detect dental caries [13]. Many studies using fluorescence spectroscopy to detect dental caries were reported. Yasser H. El-Sharkawy et al. used a 488 nm, 5 mW laser as the inducing light source and achieved precise caries removal by identifying and locating the caries location through the relevant signal processing algorithm [14]. Sung-Ae Son et al. investigated the characteristics of the fluorescence spectra of different caries stages, including slope (550 to 600 nm), spectral area (500 to 590 nm), and peak intensity ratio (625/667 nm) [12].

International Caries and Detection Assessment System II (ICDAS II) is a visual classification system developed to detect and evaluate all stages of caries development, from the initial demineralization stage to the cavitation stage [15]. The seven-point scoring system for ICDAS-II (code 0–6) gives valuable information on caries stages during dental education, clinical applications, research, and epidemiological studies [16, 17]. After the 2008 American Dental Association Symposium, it was suggested that ICDAS-II codes could be collapsed so that ICDAS-II code 0 represents sound tooth, codes 1 and 2 are early caries, codes 3 and 4 are moderate lesions, and codes 5 and 6 represent extensive lesions [18]. Tooth specimens were classified into four stages according to ICDAS-II criteria: ICDAS-II 0, ICDAS-II 1,2, ICDAS-II 3,4, and ICDAS-II 5,6, respectively.

Hyperspectral imaging is an emerging, fast and nondestructive detection technology that organically integrates traditional spectral analysis with image processing to obtain both continuous spectral information for each pixel point on the image and continuous image information for each spectral band, which can fully reflect the subtle changes in the spectral information of the sample [19]. By providing accurate spectral information related to disease conditions, hyperspectral imaging has the potential to improve the field of medical diagnosis and clinical research [20]. There have already been studies applying hyperspectral techniques to dental disease surveillance. Yasser H. El-Sharkawy et al. employed a hyperspectral camera to acquire the reflected and emitted spectra of the specimens to generate multispectral images [21]. Ahmed L. Abdel Gawad et al. proposed a set of estimated wavelengths for dental diseases using hyperspectral imaging, providing dentists with a potential diagnostic tool for evaluation [3].

Evaluation and diagnosis of dental caries by fluorescence spectroscopy is relatively common, but it is difficult to achieve miniaturization, portability, and low cost of spectral analysis devices concurrently. Fluorescence imaging exploits the chromatic aberration of different caries stages to achieve the caries classification and some commercial detection instruments are available [22–24]. Numerous related research work has been done by Qingguang Chen et al. [25–27]. However, there is still a lack of detailed and accurate correlation methods between the spectral and chromatic features of dental caries, and the characterization in chromaticity diagram visualization has not been developed. This study reports a new method to correlate the spectral and chromatic features of dental caries and apply it to the quantitative assessment prediction of dental caries and realize its visualization in the chromaticity diagram. This technology is instrumental in developing miniaturized, portable, cost-effective caries detection devices that facilitate early caries assessment and diagnosis, as well as effective and timely intervention strategies.

2. Materials and methods

2.1. Tooth specimens

Tooth specimens were collected from the Department of Endodontics at Shanghai Stomatological Hospital, Fudan University. The procedures were carried out in accordance with the ethical principles for medical research involving human beings as specified in the Declaration of Helsinki (2013 version) of the World Medical Association. This study was approved by the appropriate institutional review board. Twenty-one tooth specimens were obtained in total. Teeth were extracted due to various oral diseases. Experienced dental clinicians classified the dental surfaces (including the medial, posterolateral, occlusal, and adjacent surfaces) of these tooth specimens for caries classification using visual inspection according to the ICDAS-II criteria. Finally, 38 tooth surfaces were obtained, and they were classified into four stages, six ICDAS-II 0, ten ICDAS-II 1,2, eight ICDAS-II 3,4, and fourteen ICDAS-II 5,6 respectively. Tooth specimens were stored in 10% formalin solution and dried at room temperature before spectral collection. The time from tooth extraction to completion of the spectral acquisition was controlled within one week.

2.2. Instrument

The schematic diagram of the experimental procedure is shown in Fig. 1. The excitation light source employed a 405 nm LED (6 W) with full width at half maximum of 15 nm. The reflectance spectrum of the LED light source (380–440 nm) and the fluorescence spectra (440–780 nm) of the tooth specimens were captured by the hyperspectral imaging camera (SR-5000, TOPCON) and displayed on the computer through a pre-installed camera software. An image cubic with 1.4 million resolution (1376 × 1024) is obtained simultaneously, which means that full spectral data (380–780 nm, 1 nm interval) are obtained for each pixel

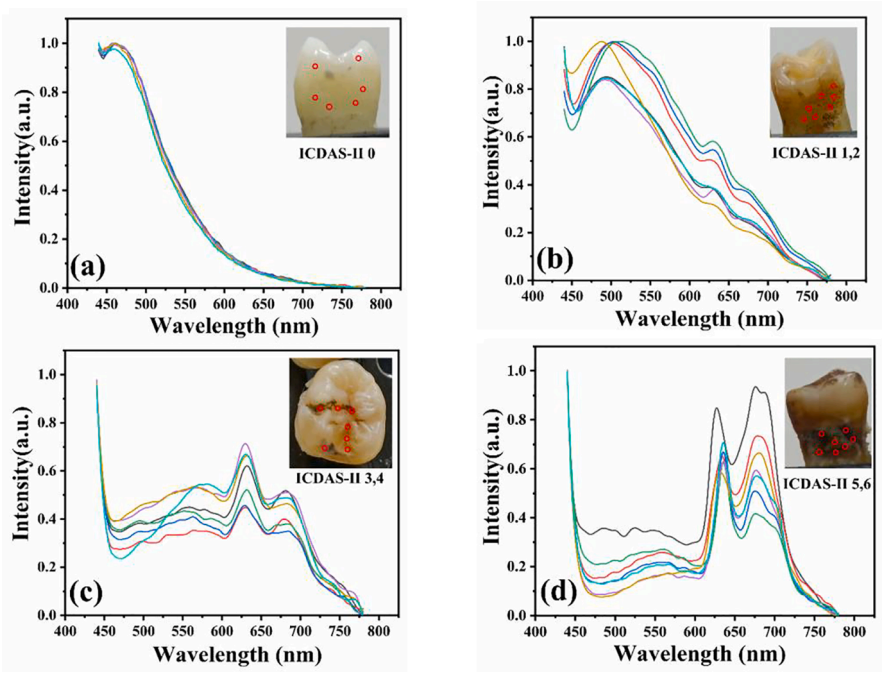

Fig. 2. Fluorescence spectra of points of interest (POIs) at four caries stages: (a) Spectra of ICDAS-II 0, (b) Spectra of ICDAS-II 1,2, (c) Spectra of ICDAS-II 3,4, (d) Spectra of ICDAS-II 5,6. The inset figures are the dental surfaces of four caries stages, and the red points are POIs.

Table 1
Number, mean, standard variance, critical interval, and statistical significance of the spectral area ratio Z for the four stages of dental caries.

Four stages of dental caries	Number of selected circular areas	*Z* mean value	*Z* standard variance	*Z* critical interval	Statistically significant (between groups)
ICDAS II 0	81	0.12	0.019	$0<Z \leq 0.15$	$p<0.001$
ICDAS II 1,2	84	0.29	0.089	$0.15<Z \leq 0.5$	$p<0.001$
ICDAS II 3,4	82	0.74	0.118	$0.5<Z \leq 1$	$p<0.001$
ICDAS II 5,6	87	1.86	0.547	$Z>1$	$p<0.001$

point. Adjust the integration time to obtain a smooth continuous spectrum. The measurements were performed in a dark room and illuminated as uniformly as possible to avoid stray light interference. With the customized camera software, the average spectral data of any region of the image can be obtained through point selection, as seen in the inset of Fig. 2. A total of 334 circular regions are selected from 38 tooth surfaces, each with a size of 3 mm. There are eighty-one ICDAS-II 0, eighty-four ICDAS-II 1,2, eighty-two ICDAS-II 3,4, eighty-seven ICDAS-II 5,6, as listed in Table 1. The custom camera software supports the selection of spectral data at any wavelength, here outputting fluorescence spectral data in the 440–780 nm band at 1 nm intervals. The output fluorescence spectral data (440–780 nm, 1 nm interval) of 334 circular regions were used as the original data set.

2.3. Statistical analysis

The spectra data of 334 circular regions were normalized. The mean value and standard variance were calculated according to four classifications (ICDAS-II 0, ICDAS-II 1,2, ICDAS-II 3,4, and ICDAS-II 5,6). Since the results (spectral area ratios, *Z*) did not meet the prerequisites of normal distribution or homogeneity of variance, the non-parametric test (Friedman) was employed here to analyze the results, as listed in Table 1. The p-value < 0.05 was considered statistically significant.

3. Results and discussion

3.1. Spectrum feature

As illustrated in Fig. 2, to obtain the spectral feature of the tooth specimens, four tooth surfaces at different stages of caries were first selected, and seven circular regions were chosen on each tooth surface image. The fluorescence spectral data (440–780 nm, 1 nm interval) of each region were acquired. The spectral trends of the various stages of caries were consistent with those in the literature [25,28], indicating that the porphyrin content of the tooth specimens was well preserved during the in-vitro process. The tooth specimens with classification level ICDAS II 0 had smooth surfaces and no significant visual alterations, and corresponding spectra were the fluorescence spectra of the enamel, with a distinct peak around 480 nm. Significant visual changes in the enamel were observed on the surfaces of tooth surface classified as ICDAS II 1,2, which were considered early caries. In addition to the fluorescence spectrum of the enamel, a smaller peak also appeared in the vicinity of 620 nm, which was the fluorescence effect produced by a small number of porphyrins. Meanwhile, the enamel showed a slight decrease and redshift from the peak position. The presence of localized enamel destruction or dark dentin shadows on the tooth surface was considered typical of dental caries and was classified as ICDAS II 3,4. The peak intensity of the enamel decreased markedly, and the fluorescence effect of the porphyrin was further increased, and the peak position began to appear at 680 nm secondarily. The decrease in peak intensity of enamel can be attributed to a decrease in fluorophore content due to structural changes [10]. The tooth surfaces classified as ICDAS II 5,6 had obvious and extensive cavities with visible dentin. The peak intensity of the enamel decreased further and emerged as strong peaks at 620 and 680 nm. In short, the disease progression of dental caries is from localized visual changes on the tooth surface to extensive cavities, and its spectral characteristics include a decreasing enamel fluorescence effect (480 nm) and an increasing porphyrin fluorescence effect (620 and 680 nm).

To obtain a universal fluorescence spectral regularity, a total of 334 circular regions were selected from the 38 tooth surfaces. 334 spectral

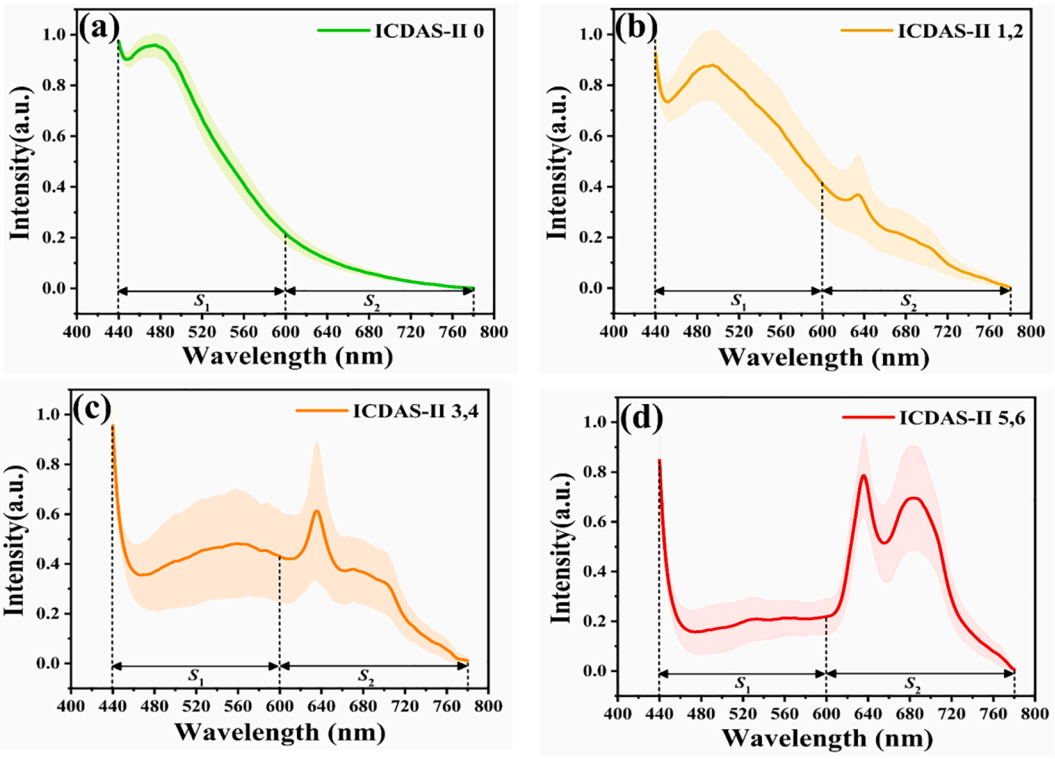

Fig. 3. Average spectra (solid line) of 334 original spectra data sets along with standard deviation (shaded area): (a) spectra of eighty-one selected circular regions for ICDAS-II 0, (b) spectra of eighty-four selected circular regions for ICDAS-II 1,2, (c) spectra of eighty-two selected circular regions for ICDAS-II 3,4, (d) spectra of eighty-seven selected circular regions for ICDAS-II 5,6.

data (440–780 nm, 1 nm interval) as the original data set were output by the camera software. The spectral data were normalized to a maximum of 1, and average spectra (solid line) along with standard deviation (shaded area) are drawn according to four caries stages, as indicated in Fig. 3. The average spectral characteristics of the four stages of caries are consistent with those discussed above. The methods of quantitative classification of caries using fluorescence spectral features include slope, area ratio, and peak ratio [10–12,27]. Due to the complexity of the oral

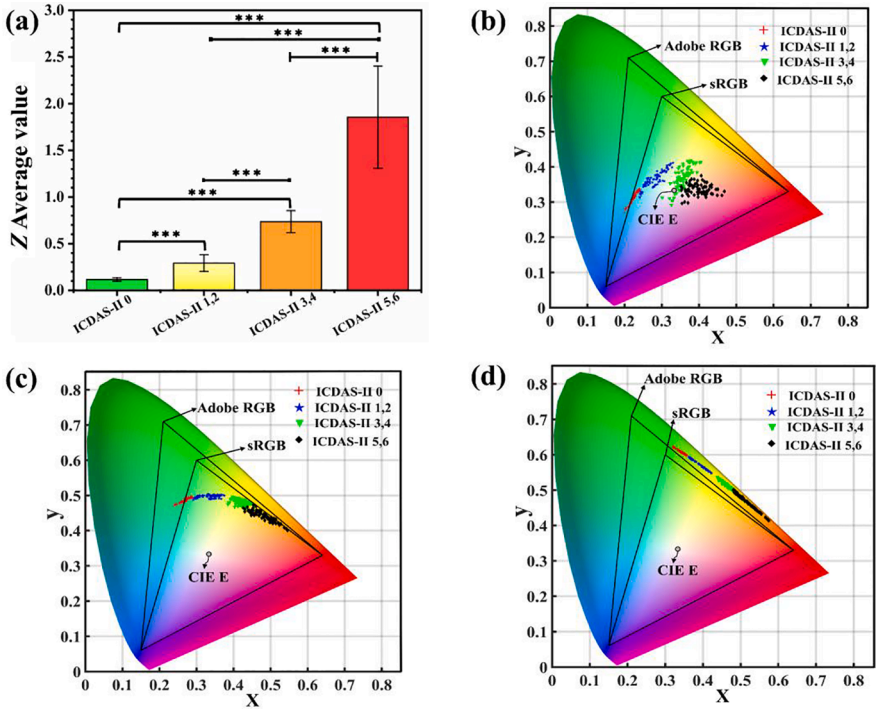

Fig. 4. (a)Mean value of *Z* for four stages of caries (with error bars), statistically significant difference was observed after the non-parametric test (Friedman, * * *$p<0.001$), (b)–(d)Visual representation of the chromaticity coordinates of four stages of caries in different wavebands after spectral matching in the CIE 1931 XYZ chromaticity diagram, (b) 440–780 nm wavebands, (c) 470–780 nm wavebands, and (d) 500–780 nm wavebands.

environment, including many types of bacteria [29], oral diseases [3] (caries, calculus), tooth surface adherence of pigments and food residues, as well as the measurement environment and the instrumentation errors, all of these can affect the results of the spectral measurement. Therefore, it is difficult to obtain the accurate spectral slope and peak ratio, and the area ratio was chosen in this work as the spectral feature for the quantitative classification of dental caries. The fluorescence effect of enamel is concentrated in the range of 440 to 599 nm, while the fluorescence effect of porphyrin content, which marks the caries stage, is mainly concentrated in the range of 600 to 780 nm. From ICDAS II 0 to ICDAS II 5,6, the fluorescence effect of tooth enamel gradually decreases while the fluorescence effect of porphyrin keeps increasing. The area ratio of the two wavebands S_1, S_2 can be applied to the discrimination of caries levels, as depicted in Fig. 3. The calculation formula is as follows:

$$Z = \frac{S_2}{S_1} = \frac{\int_{600}^{780} \varphi(\lambda) d\lambda}{\int_{440}^{599} \varphi(\lambda) d\lambda} \tag{1}$$

Where S_1 and S_2 represent the areas of the spectra in the 440–599 nm and 600–780 nm wavebands concerning the coordinate axes, respectively.

The average spectral area ratio for each caries stage was calculated using Eq. (1) after normalization for the original spectral data set, as listed in Table 1. The Z mean values are 0.12, 0.29, 0.74, and 1.86 for ICDAS II 0, ICDAS II 1,2, ICDAS II 3,4, and ICDAS II 5,6, respectively. The mean values of Z for four stages of caries (with error bars) are shown in Fig. 4(a), with statistically significant difference between groups (* * *$p<0.001$). There are clear boundaries among the four groups with no intersection or overlap. Four critical intervals for different stages of dental caries were extracted: ICDAS II 0 for Z in 0–0.15, ICDAS II 1,2 for Z in 0.15–0.5, ICDAS II 3,4 for Z in 0.5–1 and ICDAS II 5,6 for $Z>1$, as listed in Table 1.

3.2. Mapping relationships of spectral and chromatic features

In esthetic dentistry, color is widely applied to evaluate tooth restoration and whitening procedure [30]. However, few studies have been reported on the correlation between fluorescence spectral features and chromatic features for the identification of caries stages. Visible light radiation stimulates the human eye to cause color perception, and then the brain analysis to form color perception. To obtain a more consistent metric effect, the International Commission on illumination (CIE) provided a set of standard colorimetric systems [31]. The CIE chromaticity system employs three stimuli to quantitatively describe the color, from which further calculations can be obtained chromaticity coordinates [32].

The chromaticity coordinates (x, y) correspond to the color specified in the two-dimensional chromaticity diagram, as shown in Fig. 4(b)–(d). The conversion of the spectrum into color requires a specific waveband, which is generally achieved on the instrument through a customized filter. The SR-5000 camera obtained the full spectral data from 440 to 780 nm at 1 nm intervals. The original dataset contains 334 spectral data. The color perception in three different wavebands (440–780, 470–780, and 500–780 nm) is discussed here and lay the theoretical foundation for the filter selection in the later instrument development. After normalizing the 334 original data sets, the 334 chromaticity coordinates (x, y) can be obtained [32]. As seen in Fig. 4(b)–(d), 334 chromaticity coordinates (x, y) were marked with different symbols in the CIE 1931 XYZ chromaticity diagram according to the four stages of caries. 81 red plus symbols represent ICDAS II 0, 84 blue pentagram symbols represent ICDAS II 1,2, 82 green triangle symbols represent ICDAS II 3,4, and 87 black diamond symbols represent ICDAS II 5,6. The chromaticity coordinates of four caries stages obtained after matching the three wavebands spectral power distribution (SPD, 440–780, 470–780, and 500–780 nm) were distinguished from each other. As illustrated in Fig. 4(b), the chromaticity coordinates of the SPD matching in the 440–780 nm waveband were more dispersed than the other two wavebands. The color of four stages of caries transitioned from cyan to light red, while the fluorescence spectral colors of caries are blue-green (480 nm) and red (620 and 680 nm), and there is a visual difference between them. As seen in Fig. 4(c)–(d), the chromaticity coordinates of both 470–780 nm and 500–780 nm wavebands SPD matching was more aggregated. The color transitions from green to red in the four stages of dental caries, which was consistent with the caries spectral color. However, the caries detection instrument represents the color through the display, which has a certain color gamut range. sRGB and Adobe RGB are the two standard color gamut commonly applied to imaging devices and printing, respectively [33]. As seen in Fig. 4(d), the chromaticity coordinates of the SPD matching in the 500–780 nm waveband were outside the two-color gamut. Therefore, the 470–780 nm waveband SPD was chosen as the best matching color waveband, and the cutoff wavelength of the filter will be selected to be 470 nm in future instrument development. The calculation of the color aberration is further described in the supplemental document.

Table 2
The correlation coefficients (R), root mean square error (RMSE), and Fitting time of the two methods.

Method	Correlation coefficients (R)	Root mean square error (RMSE)	Fitting time/ mins
Fast Formula Fitting	0.990	0.106	30.5
Neural Network fitting	0.999	0.001	0.5

The mapping relationship between the spectral features Z and chromatic features (x, y) of dental caries was established by two methods: Fast Formula Fitting and Neural Network Fitting. The mapping relationship obtained after fast formula fitting of 334 test point data by 1stOpt software (7D-Soft High Technology Inc.) is as follows:

$$Z = p_1 + p_2x + p_3x^2 + p_4x^3 + p_5x^4 + p_6x^5 + p_7/y + p_8/y^2 + p_9/y^3 + p_{10}/y^4 + p_{11}/y^5 \tag{2}$$

Where p_1–p_{11} are −145.63, 1201.34, −6632.53, 18,049.34, −24,150.87, 12,721.90, 206.65, −145.74, −2.01, 26.84, and −5.75, respectively.

The 334 test point data were fitted with neural networks using matlab2020a software (MathWorks), of which 75% were taken as the training set, 10% as the validation set, and 15% as the test set. The correlation coefficients (R), root mean square error (RMSE), and fitting time of the two methods are listed in Table 2. All three fitting indexes of the Neural Network fitting are better than Fast Formula Fitting.

3.3. Prediction of quantitative classification of caries and visualization

The obtained mapping relationship can be applied to predict the stage of caries. Four tooth specimens of caries stages were taken as prediction specimens, and no test points were previously extracted from these four tooth surfaces. The four tooth specimens were named Specimen A, Specimen B, Specimen C, and Specimen D. The spectra of four specimens were collected by an SR-5000 camera, and seven circular areas were extracted as test points on the tooth surface of each specimen. The test points for each tooth surface are named test points 1–7, respectively. The spectral data for each test point were acquired, and data processing was carried out. The area ratio was directly obtained as Z_{EXP} using the spectral data of the test point, and the area ratio was

Table 3
The predicted results of two methods, Z_{EXP} for experimental measurements, Z_{FFF} for Fast Formula Fitting, Z_{NNF} for Neural Network fitting.

Stage of caries	Specimen A ICDAS-II 0 ($0<Z\leq 0.15$)			Specimen B ICDAS-II 1,2 ($0.15<Z\leq 0.50$)			Specimen C ICDAS-II 3,4 ($0.50<Z\leq 1$)			Specimen D ICDAS-II 5,6 (Z>1)		
	Z_{EXP}	Z_{FFF}	Z_{NNF}	Z_{EXP}	Z_{FFF}	Z_{NNF}	Z_{EXP}	Z_{FFF}	Z_{NNF}	Z_{EXP}	Z_{FFF}	Z_{NNF}
Test Point 1	0.132	0.133	0.135	0.287	0.316	0.297	0.694	0.806	0.720	1.624	2.166	1.673
Test Point 2	0.128	0.116	0.126	0.323	0.334	0.340	0.551	0.704	0.678	1.965	1.819	2.120
Test Point 3	0.131	0.118	0.129	0.449	0.455	0.455	0.544	0.617	0.629	1.682	1.773	1.924
Test Point 4	0.124	0.109	0.125	0.365	0.365	0.388	0.657	0.773	0.846	1.590	1.941	1.944
Test Point 5	0.143	0.135	0.141	0.330	0.339	0.330	0.602	0.643	0.609	1.711	1.359	1.771
Test Point 6	0.124	0.111	0.124	0.352	0.357	0.358	0.677	0.854	0.805	1.377	1.395	1.560
Test Point 7	0.131	0.131	0.134	0.360	0.360	0.371	0.643	0.775	0.778	1.356	2.166	1.353
Mean Value	0.130	0.122	0.131	0.352	0.361	0.363	0.624	0.739	0.724	1.615	1.803	1.764

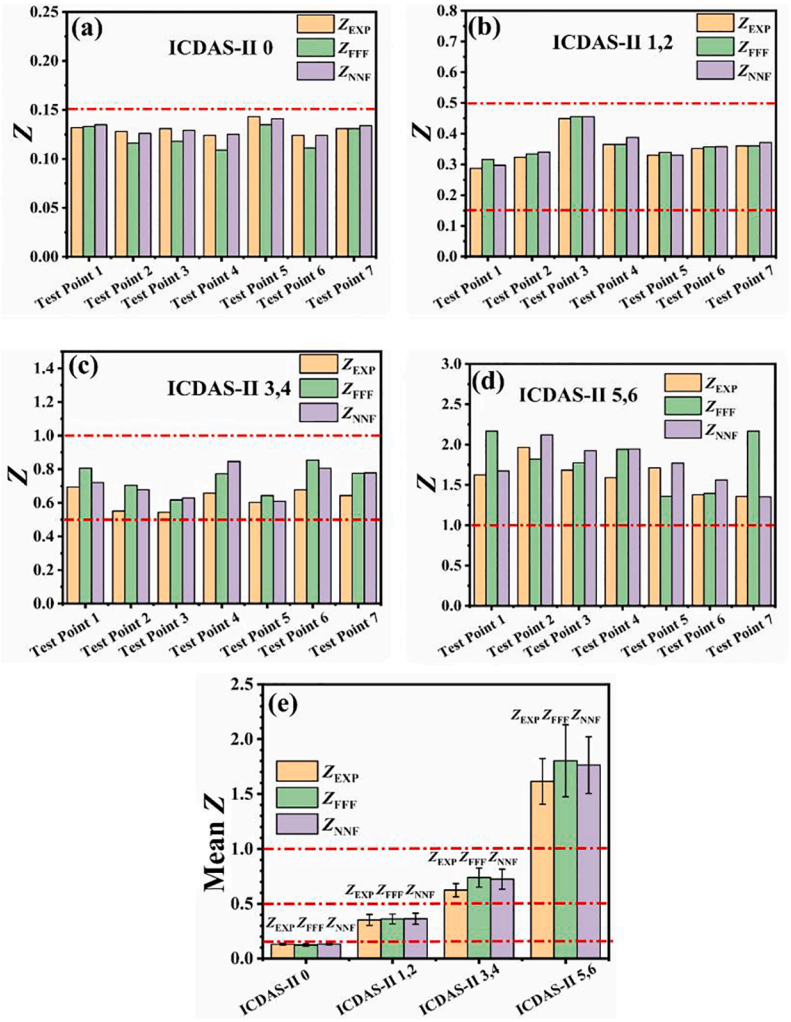

Fig. 5. The prediction results of the two methods, Z_{EXP} for experimental measurements, Z_{FFF} for fast formula fitting, and Z_{NNF} for neural network fitting: (a)-(d) for ICDAS II 0, ICDAS II 1,2, ICDAS II 3,4, and ICDAS II 5,6, respectively, (e) for the experimental mean and predicted mean of each stage. The red dashed line represents the critical value of Z.

calculated as Z_{FFF} (Fast Formula Fitting) and Z_{NNF} (Neural Network fitting) using two mapping methods after the chromaticity coordinates were obtained by SPD matching in the 470–780 nm waveband. The predicted results are given in Table 3 and Fig. 5. Both methods achieve accurate prediction of caries stages. The predicted results of 7 test points and mean values for each specimen are at the actual caries stage. Overall, the instrument only needs to obtain the chromaticity coordinates of a point or a region of the tooth surface, and Z is determined by the given mapping relationship, thus enabling the prediction of the caries stage.

Due to the advantage in R, RMSE, and fitting time, Neural Network fitting method was chosen to characterize caries stages visualized in chromaticity diagrams. Based on the chromaticity coordinate positions (Fig. 4(c)) of the 334 test points, the outline of each caries stage was determined using the four ellipses in the chromaticity diagram. Each ellipse was centered on the average chromaticity coordinates corresponding to the caries stage, and the chromaticity coordinates of the extracted test points were included in the ellipse, as shown in Fig. 6(a)-(b). The *Z* values of all chromaticity coordinates within the four ellipses were calculated using Neural Network fitting method, and the three Z

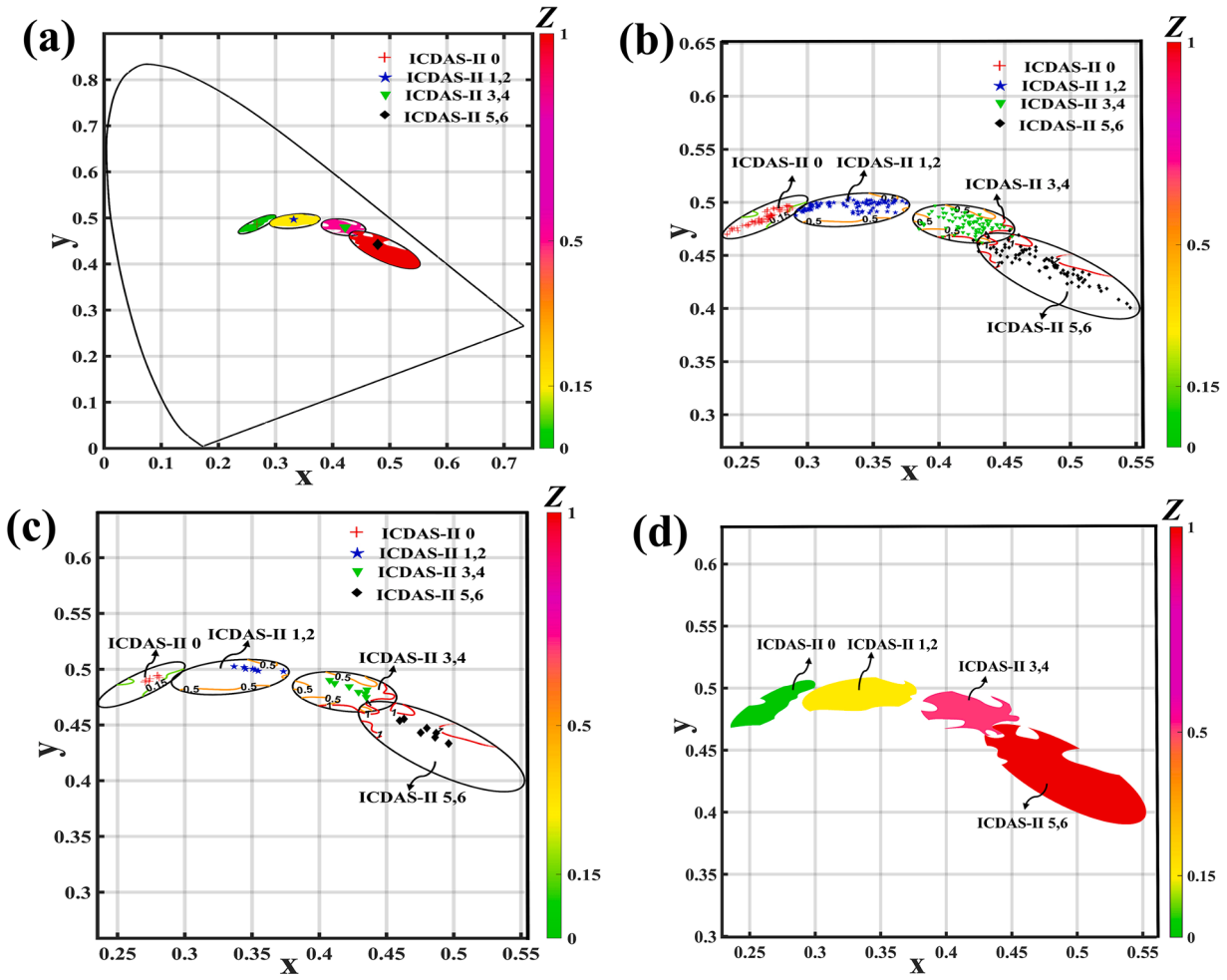

Fig. 6. (a) Four elliptical areas corresponding to different caries stages, (b) 334 test points visually characterized in the chromaticity diagram, (c) Visual representation of predicted points in the chromaticity map for four dental specimens, (d) Caries prediction area after custom color map filling.

critical values (0.15, 0.5, 1) were represented as contour lines in the chromaticity diagram. The contours of these three critical points of *Z* (0.15, 0.5, 1) and the boundaries of the ellipse together constituted the chromaticity coordinate regions of different caries stages. As presented in Fig. 6(b), the 334 test points indicating the four caries stages are all located within the corresponding regions, with only a few points falling on the boundary line, which is attributed to the fact that the *Z* values of these test points themselves are close to near the critical values. The predictive ability of the regions was verified by representing the test points of the four dental specimens for the prediction on the chromaticity diagram, as showed in Fig. 6(c). The 49 test points representing four caries stages all fell within the corresponding regions, which further validated the reliability and accuracy of the Neural Network fitting method. A set of custom colormaps was employed for region filling, and the visualized region of caries prediction was obtained in the chromaticity diagram, as seen in Fig. 6(d). The custom colormaps correspond to the spectral color of four stages of caries, and the green area represents ICDAS II 0, the yellow area represents ICDAS II 1,2, the magenta area represents ICDAS II 3,4, the red area represents ICDAS II 5,6. A rapid and accurate assessment of the caries stage can be realized by obtaining the chromaticity coordinates of measured tooth surfaces. The visual characterization of the caries stage was also achieved simultaneously, according to the position of the chromaticity coordinates in the chromaticity diagram. Since the chromaticity coordinates of most areas within each ellipse were verified to correspond to the same caries stage, the regions using the ellipse was sufficiently suitable for a simple caries stage assessment. As the number of specimens for neural network fitting increases, the range of elliptical regions will become more accurate.

4. Conclusion

A new method to correlate the spectral features of caries with chromatic features was proposed and applied to the quantitative classification prediction of dental caries and its visualization in the chromaticity diagram. A 405 nm LED light source was employed as the excitation light source. The spectral data of the 334 test points were obtained as the original data set by hyperspectral imaging camera. The area ratio of the fluorescence spectra in different wavebands (440–599 nm and 600–780 nm) was applied as a spectral feature to distinguish different caries stages. The chromaticity coordinates of the 334 test points after SPD matching in the 470–780 nm waveband fell within the common color gamut. This result provided a theoretical basis for the selection of filters for future dental caries detection instruments. The mapping relationship between caries spectral and chromatic features was obtained by fast formula fitting and neural network fitting methods. Both methods were applied to caries prediction, and achieve accurate prediction results at the pixel level. The neural network fitting approach was chosen to achieve a visual representation of caries predictions in chromaticity diagrams. All 49 test points for caries stage prediction fell within the corresponding regions, demonstrating the reliability of the obtained caries prediction regions. The caries prediction visualization area was obtained after being filled with a custom color map. The results of this work provide a theoretical foundation for the development of portable, miniaturized, low-cost caries detection instruments.

Author contributions

Cheng Wang was involved in conceptualization, methodology, formal analysis, investigation, visualization, and writing—original draft. Rongjun Zhang was involved in supervision, and project administration. Yongfu Jiang, Jiayang Li, and Nizhou Liu was involved in resources. Le Wang, Peiyu Wu, and Junbo He was involved in formal analysis, data curation. Qi Yao was involved in conceptualization, validation, writing—review and editing, supervision, project administration, and funding acquisition. Xiaoling Wei was involved in validation, resources, funding acquisition.

Data availability statement

The data that support the findings of this study are available on request from the corresponding author. The data are not publicly available due to privacy or ethical restrictions.

Declaration of Competing Interest

There are no conflicts to declare.

Acknowledgments

This work was financially supported by State Key Laboratory of Applied Optics [SKLAO2021001A16]; Jihua Laboratory Projects of Guangdong Province [X190111UZ190]; Medical Engineering Fund of Fudan University [yg2021–028].

Supplementary materials

Supplementary material associated with this article can be found, in the online version, at doi:10.1016/j.pdpdt.2021.102711.

References

[1] N.B. Pitts, D.T. Zero, P.D. Marsh, K. Ekstrand, J.A. Weintraub, F. Ramos-Gomez, J. Tagami, S. Twetman, G. Tsakos, A. Ismail, Dental caries, Nat. Rev. Dis. Primers 3 (2017) 17030, https://doi.org/10.1038/nrdp.2017.30.
[2] R.H. Selwitz, A.I. Ismail, N.B. Pitts, Dental caries[J], The Lancet, 369 (9555) (2007) 51–59, https://doi.org/10.1016/S0140-6736(07)60031-2.
[3] A.L. Abdel Gawad, Y. El-Sharkawy, H.S. Ayoub, A.F. El-Sherif, M.F. Hassan, Classification of dental diseases using hyperspectral imaging and laser induced fluorescence, Photodiagn. Photodyn. Ther. 25 (2019) 128–135, https://doi.org/10.1016/j.pdpdt.2018.11.017.
[4] F. Tetschke, L. Kirsten, J. Golde, J. Walther, R. Galli, E. Koch, C. Hannig, Application of optical and spectroscopic technologies for the characterization of carious lesions in vitro, Biomed. Eng./Biomedizinische Technik 63 (2018) 595–602, https://doi.org/10.1515/bmt-2017-0133.
[5] A.C. Ribeiro Figueiredo, C. Kurachi, V.S. Bagnato, Comparison of fluorescence detection of carious dentin for different excitation wavelengths, Caries Res 39 (2005) 393–396, https://doi.org/10.1159/000086846.
[6] H.-.E. Kim, B.-.I. Kim, Early caries detection methods according to the depth of the lesion: An in vitro comparison, Photodiagn. Photodyn. Ther. 23 (2018) 176–180, https://doi.org/10.1016/j.pdpdt.2018.06.014.
[7] N. Abogazalah, M. Ando, Alternative methods to visual and radiographic examinations for approximal caries detection, J. Oral Sci. 59 (2017) 315–322, https://doi.org/10.2334/josnusd.16-0595.
[8] N. Miyamoto, T. Adachi, F. Boschetto, M. Zanocco, T. Yamamoto, E. Marin, S. Somekawa, R. Ashida, W. Zhu, N. Kanamura, I. Nishimura, G. Pezzotti, Molecular fingerprint imaging to identify dental caries using Raman spectroscopy, Materials 13 (2020) 4900, https://doi.org/10.3390/ma13214900.
[9] J. Guo, Y. Rao, W. Zhang, Z. Cui, A. Liu, Y. Yan, Dental imaging with near-infrared transillumination using random fiber laser, Photonic Sens. 10 (2020) 333–339, https://doi.org/10.1007/s13320-020-0582-5.
[10] S.P. Singh, P. Fält, I. Barman, A. Koistinen, R.R. Dasari, A.M. Kullaa, Objective identification of dental abnormalities with multispectral fluorescence imaging, J. Biophoton. 10 (2017) 1279–1286, https://doi.org/10.1002/jbio.201600218.
[11] A. Ribeiro, C. Rousseau, J. Girkin, A. Hall, R. Strang, C.John Whitters, S. Creanor, A.S.L. Gomes, A preliminary investigation of a spectroscopic technique for the diagnosis of natural caries lesions, J. Dent. 33 (2005) 73–78, https://doi.org/10.1016/j.jdent.2004.08.006.
[12] S.-.A. Son, K.-.H. Jung, C.-.C. Ko, Y.H. Kwon, Spectral characteristics of caries-related autofluorescence spectra and their use for diagnosis of caries stage, J. Biomed. Opt. 21 (2016), 015001, https://doi.org/10.1117/1.JBO.21.1.015001.
[13] Y.-.J. Yan, B.-.W. Wang, C.-.M. Yang, C.-.Y. Wu, M. Ou-Yang, Autofluorescence detection method for dental plaque bacteria detection and classification: example of porphyromonas gingivalis, Aggregatibacter actinomycetemcomitans, and Streptococcus mutans, Dent. J. 9 (2021) 74, https://doi.org/10.3390/dj9070074.
[14] Y.H. El-Sharkawy, S. Elbasuney, Tunable laser-induced fluorescence with signal correlation algorithm for dental caries detection with controlled ablation, Opt. Laser Technol. 129 (2020), 106299, https://doi.org/10.1016/j.optlastec.2020.106299.
[15] F. Yanikoglu, H. Avci, Z.C. Celik, D. Tagtekin, Diagnostic performance of ICDAS II, FluoreCam and ultrasound for flat surface caries with different depths, Ultrasound Med. Biol. 46 (2020) 1755–1760, https://doi.org/10.1016/j.ultrasmedbio.2020.03.007.
[16] A. Jablonski-Momeni, V. Stachniss, D.N. Ricketts, M. Heinzel-Gutenbrunner, K. Pieper, Reproducibility and accuracy of the ICDAS-II for detection of occlusal caries in vitro, Caries Res 42 (2008) 79–87, https://doi.org/10.1159/000113160.
[17] B. Dikmen, ICDAS II criteria (international caries detection and assessment system), J. Istanbul Univ. Fac. Dent. 49 (2015) 63, https://doi.org/10.17096/jiufd.38691.
[18] A. Jablonski-Momeni, D.N.J. Ricketts, K. Weber, O. Ziomek, M. Heinzel-Gutenbrunner, H.M. Schipper, R. Stoll, K. Pieper, Effect of different time intervals between examinations on the reproducibility of ICDAS-II for occlusal caries, Caries Res 44 (2010) 191–195, https://doi.org/10.1159/000314674.
[19] G. Lu, B. Fei, Medical hyperspectral imaging: a review, J. Biomed. Opt. 19 (2014), 010901, https://doi.org/10.1117/1.JBO.19.1.010901.
[20] M.A. Calin, S.V. Parasca, D. Savastru, D. Manea, Hyperspectral imaging in the medical field: present and future, Appl. Spectrosc. Rev. 49 (2014) 435–447, https://doi.org/10.1080/05704928.2013.838678.
[21] Y.H. El-Sharkawy, S. Elbasuney, Laser induced fluorescence with 2-D Hilbert transform edge detection algorithm and 3D fluorescence images for white spot early recognition, Spectrochim. Acta Part A 240 (2020), 118616, https://doi.org/10.1016/j.saa.2020.118616.
[22] E. Betrisey, N. Rizcalla, I. Krejci, S. Ardu, Caries diagnosis using light fluorescence devices: VistaProof and DIAGNOdent, Odontology 102 (2014) 330–335, https://doi.org/10.1007/s10266-013-0105-6.
[23] M. Melo, A. Pascual, I. Camps, Á. del Campo, J. Ata-Ali, Caries diagnosis using light fluorescence devices in comparison with traditional visual and tactile evaluation: a prospective study in 152 patients, Odontology 105 (2017) 283–290, https://doi.org/10.1007/s10266-016-0272-3.
[24] M.B. Diniz, P.H. Campos, S. Wilde, R.de C.L. Cordeiro, A.G.F. Zandona, Performance of light-emitting diode device in detecting occlusal caries in the primary molars, Lasers Med. Sci. 34 (2019) 1235–1241, https://doi.org/10.1007/s10103-019-02717-4.
[25] Q. Chen, H. Zhu, Y. Xu, B. Lin, H. Chen, Discrimination of dental caries using colorimetric characteristics of fluorescence spectrum, Caries Res 49 (2015) 401–407, https://doi.org/10.1159/000381961.
[26] Q. Chen, X. Jin, H. Zhu, H.S. Salehi, K. Wei, 3D distribution of dental plaque on occlusal surface using 2D-fluorescence-image to 3D-surface registration, Comput. Biol. Med. 123 (2020), 103860, https://doi.org/10.1016/j.compbiomed.2020.103860.
[27] Q.G. Chen, H.H. Zhu, Y. Xu, B. Lin, H. Chen, Quantitative method to assess caries via fluorescence imaging from the perspective of autofluorescence spectral analysis, Laser Phys 25 (2015), 085601, https://doi.org/10.1088/1054-660X/25/8/085601.
[28] M.-A.I. Timoshchuk, J.S. Ridge, A.L. Rugg, L.Y. Nelson, A.S. Kim, E.J. Seibel, Real-time Porphyrin Detection in Plaque and caries: a Case Study, San Francisco, California, United States, 2015, p. 93060C, https://doi.org/10.1117/12.2081016, in: P. Rechmann, D. Fried (Eds.).
[29] N. Takahashi, B. Nyvad, The role of bacteria in the caries process: ecological perspectives, J. Dent. Res. 90 (2011) 294–303, https://doi.org/10.1177/0022034510379602.
[30] M. Melgosa, J. Ruiz-López, C. Li, P.A. García, A.Della Bona, M.M. Pérez, Color inconstancy of natural teeth measured under white light-emitting diode illuminants, Dent. Mater. 36 (2020) 1680–1690, https://doi.org/10.1016/j.dental.2020.10.001.
[31] J. Schanda, International Commission on Illumination, eds.. Colorimetry: Understanding the CIE system, CIE/Commission Internationale De L'eclairage, Wiley-Interscience, [Vienna, Austria] : Hoboken, N.J, 2007.
[32] D. Malacara, Color Vision and colorimetry: Theory and Applications, 2nd ed, SPIE, Bellingham, Wash, 2011.
[33] H.S. Chen, T.T. Chang, Color conversion technology of four-primary color images developed on wide color gamut red, green, blue monitor[J], J. Imaging Sci. Technol. 53 (6) (2009), https://doi.org/10.2352/J.ImagingSci.Technol.2009.53.6.060502, 60502-1-60502-10.